J|A|C|S
ARTICLES
Published on Web 09/01/2004

H−Bonding Patterns in the Platinated Guanine−Cytosine Base Pair and Guanine−Cytosine−Guanine−Cytosine Base Tetrad: an Electron Density Deformation Analysis and AIM Study

Jiande Gu,*,† Jing Wang,‡ and Jerzy Leszczynski*,‡

Contribution from the Drug Design & Discovery Center, State Key Laboratory of Drug Research, Shanghai Institute of Materia Medica, Shanghai Institutes for Biological Sciences, Chinese Academy of Sciences, Shanghai 200031 P. R. China, and Computational Center for Molecular Structure and Interactions, Department of Chemistry, Jackson State University, Jackson, Mississippi 39217

Received February 12, 2004; Revised Manuscript Received June 25, 2004; E-mail: jerzy@ccmsi.us;jiandegush@go.com.

Abstract: The atoms in molecule theory (AIM) and electronic structure analysis are applied together to investigate H-bonding patterns in metalated nucleobase complexes. The influence of Pt on the intra GC base pair H-bonding has been found to reduce intra base pair H-bonding of N4(C)···O6(G) in the platinated GC pair and GCGC tetrad. The relaxation of geometry constrains in metalated nucleobases is found to be decisively important in the formation of novel molecular architectures from nucleobases and metal entities. The incorporation of the platinum in the GCGC tetrad benefits the formation of the unique CH···N (H5-(C)···N1(G)) hydrogen bond pattern in the tetrad by offering improved geometric constraints rather than through changing the electronic properties around the H5(C) and N1(G) sites. Platination at the N7 of guanine reduces the deprotonation energy considerably.

Introduction

Multiple H-bonding has been found to be the driving force in the molecular recognition process in metal nucleobase complexes.[1] The interaction of nucleic acid bases with metal cations has a strong effect on the structures and properties of nucleic acids. Replacement of the protons involved in H-bonds between nucleobases by metal entities has led to compounds potentially relevant to biology and medicine.[2−8] Construction of new complexes that exploit the right angles formed by metal-N(1) and metal-N(7) purine vectors has led to novel molecular architectures for nucleobases and metal entities that include triplets,[10,11,14] tetrads,[7,8,9,12,17,18] hexagons,[13,19] molecular boxes,[13,17] and self-assembled nucleobase aggregates.[14−16] It has been recognized that Pt(II) is of great importance in the formation of these nucleobase ensembles.[7−19] H-bonding directed self-association may take place when two nucleobases are crosslinked by *trans*-a_2Pt(II).[18,19]

A detailed knowledge of the H-bonding patterns in the metalated base pair and the base tetrad is important for understanding the influence of the metal moiety on such units. It is also crucial for the development of the new designed metalated nucleobase ensembles that are relevant to biological systems. Theoretical studies have been performed at different levels to explore the effect of metals on the formation of nucleobase pairs and trimers.[11,20−31] The results obtained for

* To whom correspondence should be addressed. Phone: (601) 979-7824. Fax: (601) 979-7823.
† Shanghai Institutes for Biological Sciences.
‡ Jackson State University.

(1) Navarro, J. A. R.; Freisinger, E.; Lippert, B. *Inorg. Chem.* **2000**, *39*, 2301−2305.
(2) Sundaralingam, M.; Carrabine, J. A. *J. Mol. Biol.* **1971**, *61*, 287.
(3) Brabec, V.; Sip, M.; Leng, M. *Biochemistry* **1993**, *32*, 11676.
(4) Krizanovic, O.; Sabat, M.; Beyerle-Pfnur, R.; Lippert, B. *J. Am. Chem. Soc.* **1993**, *115*, 5538.
(5) Dalbies, R.; Leng, M. *Proc. Natl. Acad. Sci. U.S.A.* **1994**, *91*, 8147.
(6) Colombier, C.; Lippert, B.; Leng, M. *Nucleic Acids Res.* **1996**, *24*, 4519.
(7) Metzger, S.; Lippert, B. *J. Am. Chem. Soc.* **1996**, *118*, 12467−12468.
(8) Sigel, R. K. O.; Freisinger, E.; Metzger, S.; Lippert, B. *J. Am. Chem. Soc.* **1998**, *120*, 12000−12007.
(9) Luth, M. S.; Freisinger, E.; Glahe, F.; Muller, J.; Lippert, B. *Inorg. Chem.* **1998**, *37*, 3195−3203.
(10) Sigel, R. K. O.; Sabat, M.; Freisinger, E.; Mower, A.; Lippert, B. *Inorg. Chem.* **1999**, *38*, 1481−1490.
(11) Dieter-Wurm, L.; Sabat, M.; Lippert, B. *J. Am. Chem. Soc.* **1992**, *114*, 357.
(12) Luth, M. S.; Freisinger, E.; Glahe, F.; Muller, J.; Lippert, B. *Inorg. Chem.* **1998**, *37*, 5044.
(13) Rauter, H.; Mutikainen, I.; Blomberg, M.; Lock, C. J. L.; Amo-Ochoa, P.; Freisinger, E.; Randaccio, L.; Zangrando, E.; Chiarparin, E.; Lippert, B. *Angew. Chem., Int. Ed. Engl.* **1997**, *36*, 1296.
(14) Schroder, G.; Lippert, B.; Sabat, M.; Lock, C. J. L.; Faggiani, R.; Song, B.; Sigel, H. *J. Chem. Soc., Dalton Trans.* **1995**, 3767.
(15) Meiser, C.; Freisinger, E.; Lippert, B. *J. Chem. Soc., Dalton Trans.* **1998**, 2059.
(16) Witkowski, H.; Freisinger, E.; Lippert, E. *Chem. Commun*. **1997**, 1315.
(17) Rauter, H.; Hillgeris, E. C.; Erxleben, A.; Lippert, B. *J. Am. Chem. Soc.* **1994**, *116*, 616.
(18) Freisinger, E.; Rother, I. B.; Luth, M. S.; Lippert, B. *Proc. Natl. Acad. Sci. U.S.A.* **2003**, *100*, 3748−3753.
(19) Navarro, J. A.; Freisinger, E.; Lippert, B. *Inorg. Chem.* **2000**, *39*, 1059−1065.
(20) Sponer, J. E.; Leszczynski, J.; Glahe, F.; Lippert, B.; Sponer, J. *Inorg. Chem*. **2001**, *40*, 3269−3278.
(21) Sponer, J. E.; Glahe, F.; Leszczynski, J.; Lippert, B.; Sponer, J. *J. Phys. Chem. B* **2001**, *105*, 12171−12179.
(22) Sponer, J.; Sponer, J. E.; Gorb, L.; Leszczynski, J.; Lippert, B. *J. Phys. Chem. A* **1999**, *103*, 11406−11413.
(23) Sponer, J.; Sabat, M.; Gorb, L.; Leszczynski, J.; Lippert, B.; Hobza, P. *J. Phys. Chem. B* **2000**, *104*, 7535−7544.

the platinated GGC triplet (calculated at the HF level) suggest a flattened structure due to the intramolecular H-bonding interaction.[11] The protonation energy of platinated adenine has been studied at the density functional theory (DFT) level.[20] The rotation energy barrier of *trans*-$[Pt(NH_3)_2(C-N3)_2]^{2+}$ has been investigated with the DFT method.[21] The stability enhancement of base pairs through the polarization of the purine base by cations has been suggested by both the HF and DFT level studies.[22,23] Recently, a quantum chemical study suggested that the inter GC pair proton transfer is increased by the presence of divalent cations.[31]

The dimerization of Pt(II)-coordinated Guanine−Cytosine (GC) base pairs {*trans*-$[(NH_3)_2Pt(9\text{-}EtG-N7)(1\text{-}MeC-N3)]^+$} yields a metalated GCGC base tetrad.[7,8] The biological importance of this metal-coordinated base tetrad is that it resembles the guanine−cytosine−guanine−cytosine tetrad that leads to four-stranded structures important in biology.[32−35] Two unique features that are of general interest in DNA chemistry can be seen from the platinated GCGC base tetrad. The first one is that the crystal structure of this platinum-modified base tetrad reveals the unique multicenter H-bonding pattern around guanine O(6) that is strongly affected by the presence of the platinium.[8] The influence of the metals on the neighboring H-bonds is crucial in building a stable molecular assembly from metal-coordinated nucleobases. The second feature is that this compound contains an unprecedented H-bonding pattern between deprotonated guanine and neutral cytosine that involves cytosine H(5) and guanine N(1). This extends the list of H-bond types to CH···N.[7,8] Such a feature could be very important in DNA chemistry because it expands the possible H-bonding patterns in DNA base pairing interactions.

In this paper, our attention is focused on the electronic density characteristics of the unusual H-bonding patterns of the platinated GC base pairs (*trans*-$[(NH_3)_2Pt(GH-N7)(C-N3)]^{2+}$ and *trans*-$[(NH_3)_2Pt(G-N7)(C-N3)]^+$) and the corresponding dimer {*trans*-$[(NH_3)_2Pt(G-N7)(C-N3)]^+$}$_2$. Specifically, the influence of platinum on its neighboring H-bonding pattern and the CH···N type H-bond are studied through a combined approach that uses electron density deformation analysis and the atoms-in-molecules (AIM) theory. At the electronic structure level, these electron density characteristics provide deeper insight concerning the influence of metal cations on the H-bonding between the nucleobases. Also, the deprotonation energy of the platinated GC base pair of the tetrad is evaluated. These physical properties are of vital importance to the prediction of molecular recognition in the platinated nucleobase tetrad complexes and to the development of novel molecular architectures of metal-coordinated nucleobases. It should be noted that all of the effects reported here are based on the gas phase models. Nongas phase environments might reduce some of these effects. However, the analysis of gas phase intrinsic trends is extremely valuable for understanding the basic interactions in the formation of molecular ensembles of metal-coordinated nucleobases.

Method of Calculation

The local minima of the tetrad complexes have been fully optimized by the analytic gradient techniques. The methods used were the Hartree−Fock (HF) self-consistent field approach and the density functional theory (DFT) with Becke's three parameter (B3)[36] exchange functional along with the Lee−Yang−Parr (LYP) nonlocal correlation functional (B3LYP).[37,38] The standard valence triple-ζ basis set, augmented with *d*-type and *p*-type polarization functions, 6-311G(*d*,*p*),[39] was used for all of the nonmetal elements. It is well-known that the geometries and frequencies of the species calculated at the B3LYP/6-311G(*d*,*p*) level agree well with experiment.[40] Our previous studies of hydrogen-bonded systems involving DNA bases have shown that the B3LYP approach predicts reliable interaction energies and is compatible with the MP2/6−31(*d*,*p*) method.[41,42] Three different basis sets were used for platinum to ensure reliable results. The all-electron basis set AE represents the valence double-ζ basis set [10s8p5d1f] contraction of the (17s13p8d1f) primitive set by Huzinaga[43] plus two p and one f functions for Pt. In addition, for comparison the LANL2DZ relativistic pseudopotential[44] and the small core relativistic pseudopotential MWB of the Stuttgart group[45] were used for Pt. To analyze the H-bonding pattern in the tetrads, the atoms-in-molecules (AIM) theory of Bader[46,47] was applied. The Gaussian-98 package of programs[48] was used in the calculations.

Results and Discussion

Closed-shell configuration of *trans*-$[(NH_3)_2Pt(GH-N7)(C-N3)]^{2+}$ has been optimized at the HF and DFT levels of theory with three different basis sets. The resultant structure is depicted in Figure 1, and the main geometric parameters are listed in Table 1. The optimized geometric parameters at the DFT level are similar to those optimized at the HF level except for the H-bonds between the proton of the coordinated ammonia (a1) and the O6 of guanine and between the proton of NH_3 (a2) and the O2 of cytosine. The influence of the basis sets of Pt on the geometry of the optimized complexes is insignificant.

(24) Burda, J. V.; Zeizinger, M.; Šponer, J.; Leszczynski, J. *J. Chem. Phys.* **2000**, *113*, 2224−2232.
(25) Zeizinger, M.; Burda, J. V.; Šponer, J.; Kapsa, V.; Leszczynski, J. *J. Phys. Chem. A* **2001**, *105*, 8086−8092.
(26) Burda, J. V.; Šponer, J.; Leszczynski, J. *Phys. Chem. Chem. Phys.* **2001**, *3*, 4404−4411.
(27) Burda, J. V.; Šponer, J.; Hrabáková, J.; Zeizinger, M.; Leszczynski, J. *J. Phys. Chem. B* **2003**, *107*, 5349−5356.
(28) Burda, J. V.; Leszczynski J. *Inorg. Chem.* **2003**, *42*, 7162−7172.
(29) Burda, J. V.; Zeizinger, M.; Leszczynski, J. *J. Chem. Phys.* **2004**, *120*, 1253−1262.
(30) Munoz, J.; Sponer, J.; Hobza, P.; Orozco, M.; Luque, F. J. *J. Phys. Chem. B* **2001**, *105*, 6051−6060.
(31) Noguera, M.; Bertran, J.; Sodupe, M. *J. Phys. Chem. A* **2004**, *108*, 333−341.
(32) Kettani, A.; Kumar, R. A.; Patel, D. J. *J. Mol. Biol.* **1995**, *254*, 638−656.
(33) Darlow, J. M.; Leach, D. R. F. *J. Mol. Biol.* **1998**, *275*, 3−16.
(34) Kettani, A.; Bouaziz, S.; Gorin, A.; Zhao, H.; Jones, R. A.; Patel, D. J. *J. Mol. Biol.* **1998**, *282*, 619−636.
(35) Leonard, G. A.; Zhang, S.; Peterson, M. R.; Harrop, S. J.; Helliwell, J. R.; Cruse, W. B. T.; Langlois, d'. Estaintot B.; Kennard, O.; Grown, T.; Hunter, W. N. *Structure* **1995**, *3*, 335−340.
(36) Becke, A. D. *J. Chem. Phys.* **1993**, *98*, 5648−5652.
(37) Lee, C.; Yang W.; Parr, R. G. *Phys. Rev. B* **1988**, *37*, 785−789.
(38) Miehlich, B.; Savin, A.; Stoll H.; Preuss, H. *Chem. Phys. Lett.* **1989**, *157*, 200−206.
(39) Hehre, W. J.; Radom, L.; Schleyer, P. R.; Pople, J. A. *Ab initio Molecular Orbital Theory*; Wiley: New York, 1986.
(40) Mebel, A. M.; Morokuma, K.; Lin, C. M. *J. Chem. Phys.* **1995**, *103*, 7414−7421.
(41) Sponer, J.; Leszczynski, J.; Hobza, P. *J. Phys. Chem.* **1996**, *100*, 1965−1974.
(42) Gu, J.; Leszczynski, J. *J. Phys. Chem. A* **1999**, *103*, 577−584.
(43) Huzinaga, S. *J. Chem. Phys.* **1977**, *66*, 4245.
(44) Hay, P. J.; Wadt, W. R. *J. Chem. Phys.* **1985**, *82*, 299.
(45) Andrae, D.; Haeussermann, U.; Dolg, M.; Stoll, H.; Preuss, H. *Theor. Chim. Acta* **1990**, *77*, 123.
(46) Bader, R. F. W. *Atoms in Molecules: a Quantum Theory*; Clarendon Press: Oxford, 1990.
(47) Bader, R. F. W. *Chem. Rev.* **1991**, *91*, 893.
(48) *Gaussian 98*, Revision D.3, Frisch, M. J.; Trucks, G. W.; Schlegel, H. B.; Gill, P. M. W.; Johnson, B. G.; Robb, M. A.; Cheeseman, J. R.; Keith, T.; Petersson, G. A.; Montgomery, J. A.; Raghavachari, K.; Al-Laham, M. A.; Zakrzewski, V. G.; Ortiz, J. V.; Foresman, J. B.; Cioslowski, J.; Stefanov, B. B.; Nanayakkara, A.; Challacombe, M.; Peng, C. Y.; Ayala, P. Y.; Chen, W.; Wong, M. W.; Andres, J. L.; Replogle, E. S.; Gomperts, R.; Martin, R. L.; Fox, D. J.; Binkley, J. S.; Defrees, D. J.; Baker, J.; Stewart, J. P.; Head-Gordon, M.; Gonzalez, C.; Pople, J. A. Gaussian, Inc., Pittsburgh, PA, 1998.

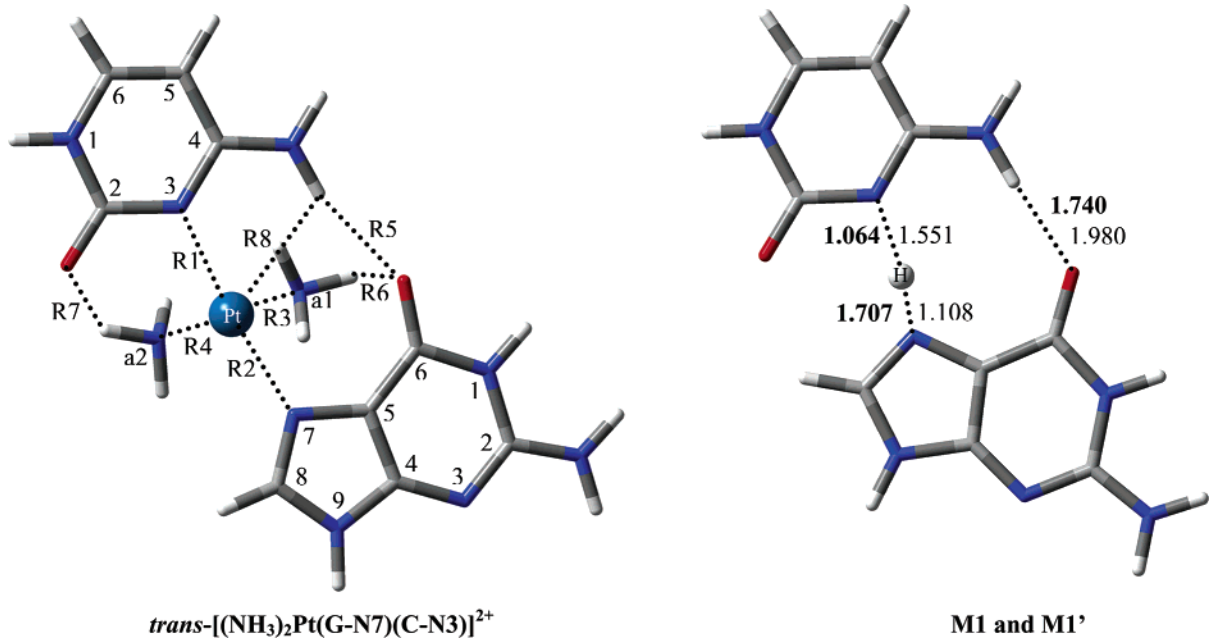

Figure 1. Optimized structure of the platinated GC pair ***trans*-[(NH$_3$)$_2$Pt(GH−N7)(C−N3)]$^{2+}$** and the corresponding models **M1** and **M1′**. The representations of color at the atomic position are red for O, blue for N, gray for C, and white for H. Geometric parameters of the models are given in Å. Plain number is for **M1**, and bold is for **M1′**.

Table 1. Optimized Geometric Parameters of *trans*-[(NH$_3$)$_2$Pt(GH−N7)(C−N3)]$^{2+}$ (I), the Deprotonated Complex *trans*-[(NH$_3$)$_2$Pt(G−N7)(C−N3)]$^{+}$ (II), and {*trans*-[(NH$_3$)$_2$Pt(G−N7)(C−N3)]$^{+}$}$_2$ (III) at the B3LYP/AE Level of Theory[a]

	I	II	III	IV
		atomic distance		
R1: N3(C)···Pt	2.143	2.158	2.146	2.024
R2: N7(G)···Pt	2.139	2.114	2.117	2.008
R3: N(a1)···Pt	2.168	2.159	2.158	
R4: N(a2)···Pt	2.161	2.166	2.166	
R5: H4(C)···O6(G)	2.207	1.728	2.279 (3.243[a])	3.229[a]
R6: H(a1)···O6(G)	2.173	1.836	1.865	
R7: H(a2)···O2(C)	2.103	2.136	2.016	
R8: H4(C)···Pt	2.725	2.726	2.677	
R9: H4(C′)···O6(G)			1.770 (2.792[b])	2.715[b]
R10: H5(C′)···N1(G)			2.288 (3.333[c])	3.548[c]
		atomic angle		
N3(C)−Pt−N7(G)	172.8	168.4	172.8	178.4
N(a1)−Pt−N(a2)	176.5	177.7	178.1	
N(a1)−H−O6(G)	133.0	141.4	147.2	
N4(C)−H−O6(G)	160.8	163.2	157.7	
N4(C)−H−Pt	111.5	108.9	113.7	
N(a2)−H−O2(C)	132.3	133.4	136.1	
N4(C′)−H−O6(G)			167.1	
C5(C′)−H−N1(G)			161.3	

[a] Basis set used for nonmetal elements is 6-311G(d,p). Atomic distance in Å; atomic angle in (°). Crystallographic data of {*trans*-[(NH$_3$)$_2$Pt(9-EtG-N7)(1-MeC−N3)]$^{+}$}$_2$ are listed in IV.[8] [a] Atomic distance between N4(C) and O6(G). [b] Atomic distance between N4(C′) and O6(G). [c] Atomic distance between C5(C′) and N1(G).

The bond distances between Pt and the coordinated N predicted with the all-electron basis set are slightly longer than those with pseudo potential basis sets LANL2DZ and MWB. The average difference amounts to 0.07 Å at both the HF and DFT levels of theory. The H-bonds between the proton of the coordinated NH_3 groups (a1 and a2) and the O6 of G and O2 of C are 0.09 Å and 0.07 Å longer at the DFT/AE level as compared to those at the DFT/LANL2DZ and DFT/MWB levels, respectively. Overall, the geometric parameters predicted with the different basis sets are consistent with each other, signifying that the relativistic effects are not important for descriptions of the studied properties of this complex. This consistency can also be seen from the optimized structures of the N1(G) deprotonated complex of the platinated GC base pair (*trans*-[(NH$_3$)$_2$Pt(G−N7)(C−N3)]$^{+}$) and its dimer {*trans*-[(NH$_3$)$_2$Pt(G−N7)(C−N3)]$^{+}$}$_2$ (Figures 2, 3 and Table 1).

Geometries of the Complexes: Theoretical Predictions vs the Crystallographic Data. In general, the theoretical geometric parameters agree well with the crystallographic data.[8]

In *trans*-[(NH$_3$)$_2$Pt(GH−N7)(C−N3)]$^{2+}$, N3(C)···Pt (**R1**) and N7(G)···Pt (**R2**), the theoretically estimated bond lengths are about 0.06 to 0.13 Å longer as compared with those observed in crystal structures (2.143 Å for **R1** vs 2.024 Å and 2.139 Å for **R2** vs 2.008 Å, respectively).[8] The N4(C)···O6(G) separation of 3.00 Å and 3.11 Å measured in the crystal structures has been evaluated to be 3.184 Å in our theoretical calculations. This corresponds to a relatively larger H-bonding distance of H4(C)···O6(G) (**R5** = 2.207 Å). According to the calculations, the molecular plane of guanine is titled relative to cytosine by about 4.3°, which is in good agreement with the experimental values of 5.5° and 6.3°. The calculated value of 172.8° at the B3LYP/AE level (174.9° at the B3LYP/MWB level) for the N3(C)-Pt−N7(G) angle reproduces the experimental value of 175.0°.

The *trans*-[(NH$_3$)$_2$Pt(G−N7)(C−N3)]$^{+}$ cation is obtained from *trans*-[(NH$_3$)$_2$Pt(GH−N7)(C−N3)]$^{2+}$ by deprotonation at the N1 position of guanine (Figure 2). There are several significant differences between the geometric parameters of the deprotonated *trans*-[(NH$_3$)$_2$Pt(G−N7)(C−N3)]$^{+}$ complex (see Table 1) and its parent compound. The N3(C)−Pt−N7(G) angle decreases by approximately 5° in the former as compared with the latter. The **R5** and **R6** bond distances that are related to O6(G) are remarkably reduced (1.728 Å and 1.836 Å) due to the deprotonation. At a first glance, these changes are inconsistent with those found in experiments.[8] However, it should be noted that the crystallographic data reported are from the

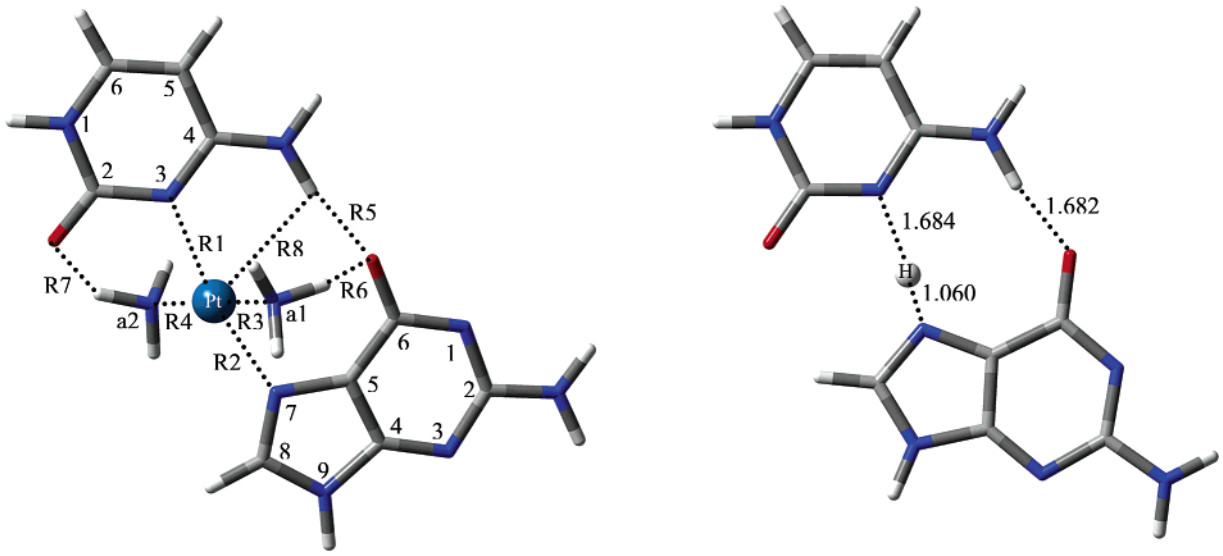

trans-$[(NH_3)_2Pt(G\text{-}N7)(C\text{-}N3)]^+$ M2

Figure 2. Optimized structure of the N1 deprotonated platinated GC pair ***trans*-$[(NH_3)_2Pt(G{-}N7)(C{-}N3)]^+$** and the corresponding model M2. The representations of color at the atomic position are red for O, blue for N, gray for C, and white for H. Geometric parameters of the models are given in Å.

dimer of the deprotonated complex.[8] In fact, as can be seen below, these geometric parameters correspond very well to the molecular geometry obtained in our calculations for the dimerized *trans*-$[(NH_3)_2Pt(G{-}N7)(C{-}N3)]^+$ complex. Therefore, a decrease in the N3(C)−Pt−N7(G) angle and the remarkable reduction of the **R5** and **R6** distances should allow for a reliable prediction of the molecular geometry of the deprotonated GC pair. Another significant change predicted for the deprotonated complex is the considerable increase of the plane angle between the G and C bases. The G−C plane angle amounts to about 15° at the B3LYP/AE level of theory. The higher propeller twist of the G and C bases is mainly the result of the deprotonation of the compound.

Although no symmetric constrains were imposed upon the initial structures of $\{$*trans*-$[(NH_3)_2Pt(G{-}N7)(C{-}N3)]^+\}_2$, the final optimized structures exhibit *Ci* symmetry. As mentioned above, good correspondence between the theoretical prediction and the crystallographic data has been noticed for the geometry of the N-platinated GCGC base tetrad $\{$*trans*-$[(NH_3)_2Pt(G{-}N7)(C{-}N3)]^+\}_2$. Specifically, the H4(C)···O6(G) bond distance has been evaluated to be 2.279 Å, which corresponds to the N4(C)···O6(G) atomic distance of 3.243 Å. As a comparison, an analogous crystallographic value amounts to 3.229 Å. The N3(C)-Pt−N7(G) bond angle is predicted to be 172.8° which is 5.6° less than the experimental value (178.4°). Considering that the calculated values relate to the isolated molecule, this underestimation of the bond angle is reasonable. Another possible reason for the underestimation of the N3(C)-Pt−N7(G) bond angle in $\{$*trans*-$[(NH_3)_2Pt(G{-}N7)(C{-}N3)]^+\}_2$ is that counterions are not included in the calculations.

Overall, good agreement as compared to the crystallographic data ensure high quality for the evaluated properties and reliability of the calculation methods used in the study.

Influence of Pt on the H4(C)···O6(G) H-Bonding Pattern. There are three H-bonds in the *trans*-$[(NH_3)_2Pt(GH{-}N7)(C{-}N3)]^{2+}$ compound: the H-bond between the proton of coordinated NH_3 (a1) and O6 of guanine (**R6**), the H-bond between the proton of NH_3 (a2) and O2 of cytosine (**R7**), and the interbase H-bond H4(C)···O6(G) (**R5**). The relatively longer H-bond length of **R6** and **R7** (2.173 Å and 2.103 Å) is clearly due to the geometric constraints on the proton donor NH_3 that corresponds to the inferior atomic angle of N(a1)−H−O6(G) and N(a2)−H−O2(C) (133.0° and 132.3° at the B3LYP/AE level). A 0.07 Å elongation of **R6** compared to **R7** could be the result of the competition from the interbase H-bond **R5.** Although the bond angle of N4(C)−H−O6(G) (160.8°) favors the interbase H-bond H4(C)···O6(G), its bond distance has been found to be even longer (2.207 Å) and is significantly longer than the typical H(C)···O6(G) H-bond in the GCGC tetrad (1.989 Å and 1.872 Å in the O-bifurcated H-bonding form).[49] Since the competition from **R6** (2.173 Å) is weaker than that from the second branch of H-bond (1.989 Å) in the GCGC tetrad, the increase of 0.22 ∼ 0.33 Å in **R5** should be the result of the influence of platinum.

To analyze the influence of platinum on the H4(C)···O6(G) H-bonding, a model system in which the $(NH_3)_2Pt^{2+}$ moiety is replaced by a proton, forming the well-known Hoogsteen GC^+ pair,[50] has been studied at the same theoretical level (B3LYP/6-311G(d,p)). The optimized structure displayed in Figure 1 shows that there are two local minima on the potential energy surface of such a complex. Depending on the position of H^+, it is labeled as **M1** when the proton is close to guanine or **M1′** when the proton is located near cytosine. **M1** has been found to be less stable (by about 3.6 kcal/mol) than **M1′**. The H4(C)···O6(G) bond length in **M1** is very close to that of the O-bifurcated H-bonding form in the GCGC tetrad (1.980 Å vs 1.989 Å).[38] Based on this model, the elongation of the H4(C)···O6(G) bond length caused by the competition of NH_3 with O6(G) in the *trans*-$[(NH_3)_2Pt(GH{-}N7)(C{-}N3)]^{2+}$ compound is estimated to be around 0.01 Å. Therefore, the influence of Pt^{2+} on the H4(C)···O6(G) bond dominates. It should be noted that the H4(C)···Pt atomic distance (**R8**) of 2.725 Å is quite

(49) Gu, J.; Leszczynski, J. *J. Phys. Chem. A* **2000**, *104*, 7353−7358.
(50) Quigley, G. J.; Ughetto, G.; van der Marel, G. A.; van Boom, J. H.; Wang, A. H. J.; Rich, A. *Science* **1986**, *232*, 1255−1258.

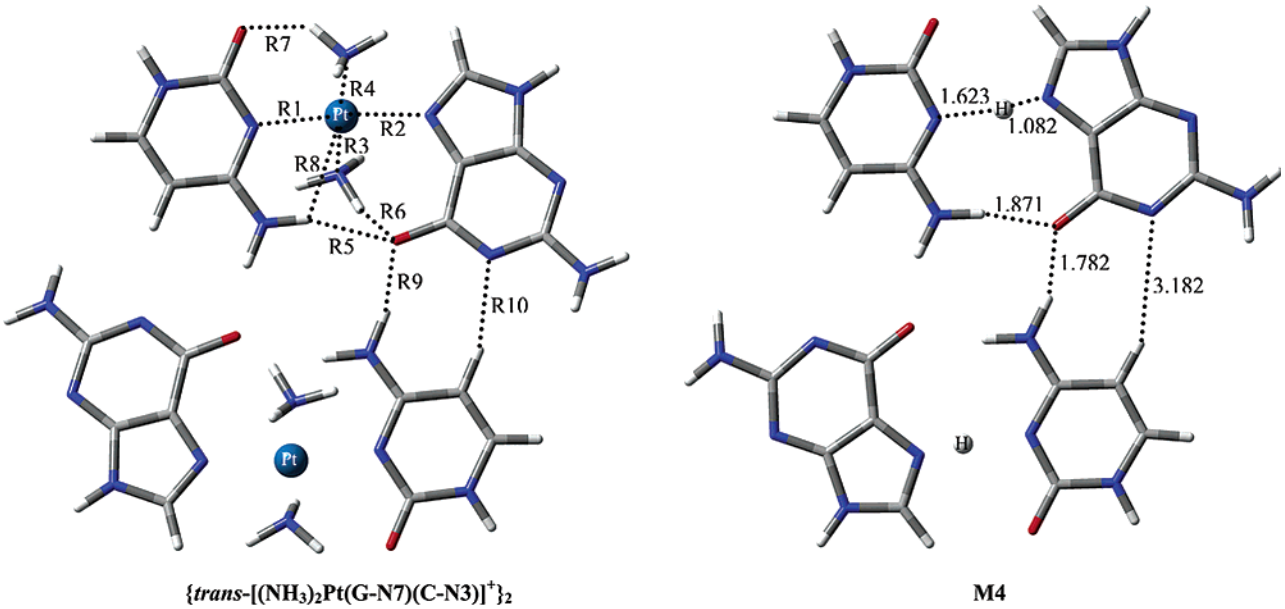

Figure 3. Optimized structures of the platinated GCGC tetrad and the corresponding model **M4**. The representations of color at the atomic position are red for O, blue for N, gray for C, and white for H. Geometric parameters of the models are given in Å.

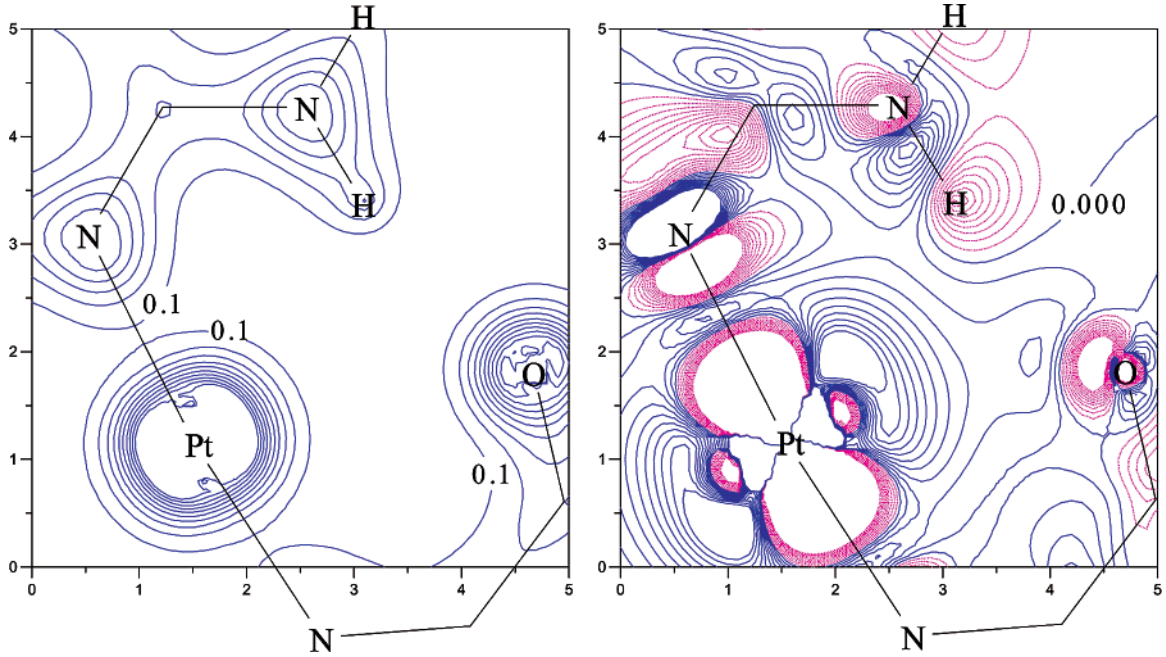

Figure 4. Electron density and the density difference ($\Delta\rho$) map in the plane of Pt−O6(G)−H4(C). The increase of contour lines in the density map is at 0.1 au. Contours in the deformation density map at ±0.001 au. Dashed pink is for decrease of density, and solid blue is for increase of density. $\Delta\rho = \rho[(NH_3)_2PtGHC^{2+}] - \rho[(NH_3)_2Pt^{2+}] - \rho[GH] - \rho[C]$.

short compared to the large radius of Pt^{2+}. Since compounds with a H-bond involving transition metals have been identified,[51−54] the weakening of the H4(C)···O6(G) H-bond could be either through the interaction between Pt^{2+} and O6 of guanine or by the formation of the H4(C)···Pt H-bond.

H-bonding can be characterized by the change of electron density for the bonded moiety. The electron density around the proton and the proton acceptor decreases, while the density between the proton and its acceptor increases as the result of the formation of a H-bond.[55] The alteration of electron density from G, C, and the $(NH_3)_2Pt^{2+}$ moiety to the *trans*-$[(NH_3)_2Pt(GH-N7)(C-N3)]^{2+}$ compound has been plotted in Figure 4. As a comparison, the deformation density map of the **M1** model complex has been depicted in Figure 5. The electronic structure of the H4(C)···O6(G) H-bond reveals itself in the deformation density map of **M1**. The concentration of electron density arises between the proton and the proton acceptor with a corresponding

(51) Brammer, L.; Channock, J. M.; Goggin, P. L.; Goodfellow, R. J.; Orpen, A. G.; Koetzle, T. *J. Chem. Soc., Dalton Trans.* **1991**, 1789−1798.
(52) Brammer, L.; McCann, M. C.; Bullock, R. M.; McMullan, R. K.; Sherwood, R. *Organometallics* **1992**, *11*, 2339−2341.
(53) Kazarian, S. G.; Hamley, P. A.; Poliakoff, M. *J. Am. Chem. Soc*. **1993**, *115*, 9069−9079.
(54) Brammer, L.; Zhao, D.; Ladipo, F. T.; Braddock-Willking, *J. Acta Cryst*. **1995**, *B51*, 632−640.
(55) Vanquickenborne, L. G. Quantum Chemistry of Hydrogen Bond. In *Intermolecular Forces*; Huyskens, P. L., Luck, W. A. P., Zeegers-Huyskens, T., Eds.; Springer-Verlag Berling: Heidelberg, 1991; p 41.

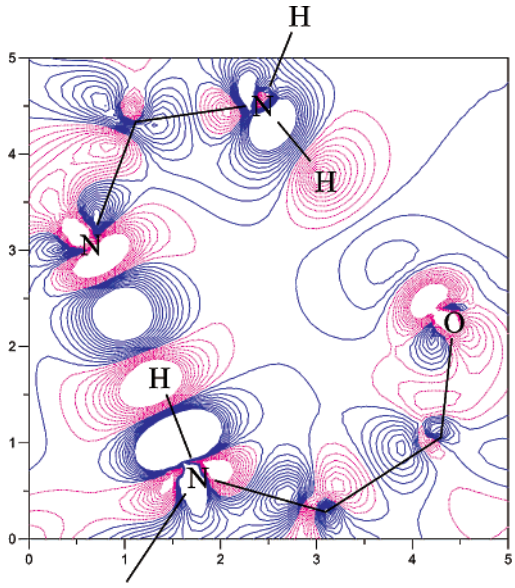

Figure 5. Electron density difference ($\Delta\rho$) map in the plane of H^+−O6(G)−H4(C) of **M1**. Contours at ±0.001 au. Dashed pink is for decrease of density, and solid blue is for increase. $\Delta\rho = \rho[GH^+C] - \rho[GH^+] - \rho[C]$.

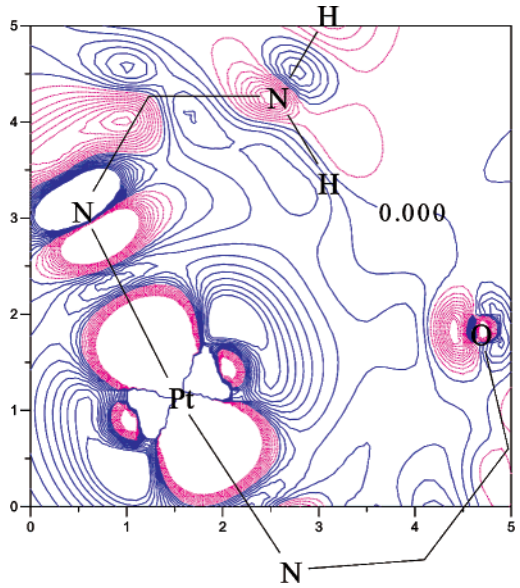

Figure 6. Density difference between the complex and the GC pair and the $(NH_3)_2Pt^{2+}$ moiety: $\Delta\rho = \rho[(NH_3)_2PtGHC^{2+}] - \rho[(NH_3)_2Pt^{2+}] - \rho[GHC]$. The electron density deformation map in the plane of Pt−O6(G)−H4(C) of the platinated GC pair. Contours at ±0.001 au. Dashed pink is for decrease of density, and solid blue is for increase of density.

electron density deficiency at the positions of a proton and the acceptor lone pair. The electron density increase along the strong H-bond (H7(G)···N3(C)) is much larger compared to that of the weaker H-bond (H4(C)···O6(G)) in **M1**. The electron density difference map of *trans*-$[(NH_3)_2Pt(GH-N7)(C-N3)]^{2+}$ (Figure 4) also exhibits a decrease in density at the proton position and at the lone electron pair of O6(G). However, the increasing electron density is transferred away from the H-bond line between H4(C) and O6(G) due to the attraction from the Pt^{2+} cation, resulting in a weak H4(C)···O6(G) H-bond. The possibility for the formation of the H4(C)···Pt H-bond can be excluded by comparing the total electron density of the complex with the summation of the individual density of the GC pair and the $(NH_3)_2Pt^{2+}$ moiety. The density difference between the complex and the GC pair and the $(NH_3)_2Pt^{2+}$ moiety in Figure 6 further demonstrates that there is no obvious electron deficiency at the location of the H4(C) proton. The main contribution of the density increase comes from Pt and O6(G) as can be seen from Figure 6. Consequently, an attractive interaction between Pt and O6(G) is expected.

The AIM theory has been proven a useful and successful tool in the interpretation of charge density toward a wide variety of chemical concepts.[38] The density at the bond critical point (BCP) is of paramount importance in AIM. It has been used to characterize different types of chemical bonds. In this study, the AIM calculations were performed at the B3LYP/AE level of theory. The charge densities of BCPs around Pt and H4(C)···O6(G) along with those of the model **M1** complex have been depicted in Figure 7. The large value (0.022 au) of the density at the BCP of the H4(C)···O6(G) bond in **M1** is consistent with its short bond length and the well-defined electronic structure discussed above. Meanwhile, the small BCP density value of 0.013 au for the H4(C)···O6(G) bond in *trans*-$[(NH_3)_2Pt(GH-N7)(C-N3)]^{2+}$ is in accordance with the weak H-bond as a result of the influence of Pt^{2+}. The attraction between Pt^{2+} and O6(G) expected from the electronic structure analysis is confirmed by the AIM analysis. The bond critical

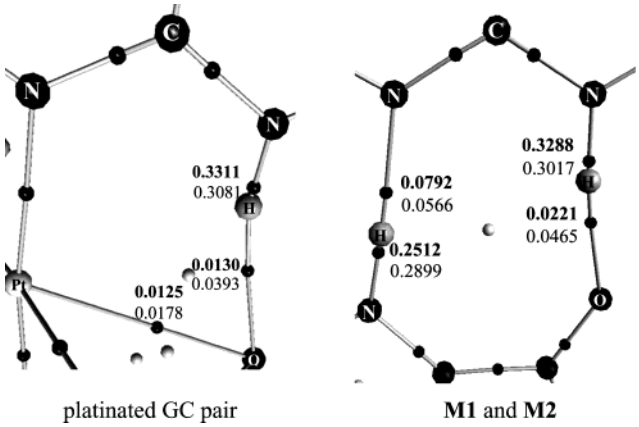

Figure 7. Density of bond critical points around the H4(C)···O6(G) H-bond and Pt in the platinated GC pair and the corresponding models. The unit of density is in au. Numbers in bold are for *trans*-$[(NH_3)_2Pt(GH-N7)(C-N3)]^{2+}$ and **M1**; in plain are for *trans*-$[(NH_3)_2Pt(G-N7)(C-N3)]^{+}$ and **M2**. A bond path and a BCP can be seen between Pt and O6(G) for the platinated GC pairs.

point has been found between Pt^{2+} and O6(G) with the density of 0.0125 au. The suggestion that the interbase H-bonding between G and C is weakened mainly due to the competition interaction between Pt^{2+} and O6(G) is also confirmed.

Influence of the N1(G) Deprotonation on the H4(C)··· O6(G) H-Bonding Pattern. As mentioned above, the **R5** and **R6** bond distances that are related to O6(G) are remarkably reduced (1.728 Å and 1.836 Å) due to the deprotonation of the platinated GC base pair. As a comparison, the N1(G) deprotonated complex (**M2**) of the model compound **M1** has also been optimized at the B3LYP/6-311G(d,p) level of theory (Figure 2). In accord with the change in monovalenced *trans*-$[(NH_3)_2Pt(G-N7)(C-N3)]^{+}$, the H4(C)···O6(G) H-bond in **M2** is reduced to 1.682 Å, about 0.30 Å shorter than that in **M1**.

The characteristics of the H4(C)···O6(G) H-bond revealed in the deformation density map of *trans*-$[(NH_3)_2Pt(G-N7)(C-N3)]^{+}$ exhibit a well-defined electron density increase between

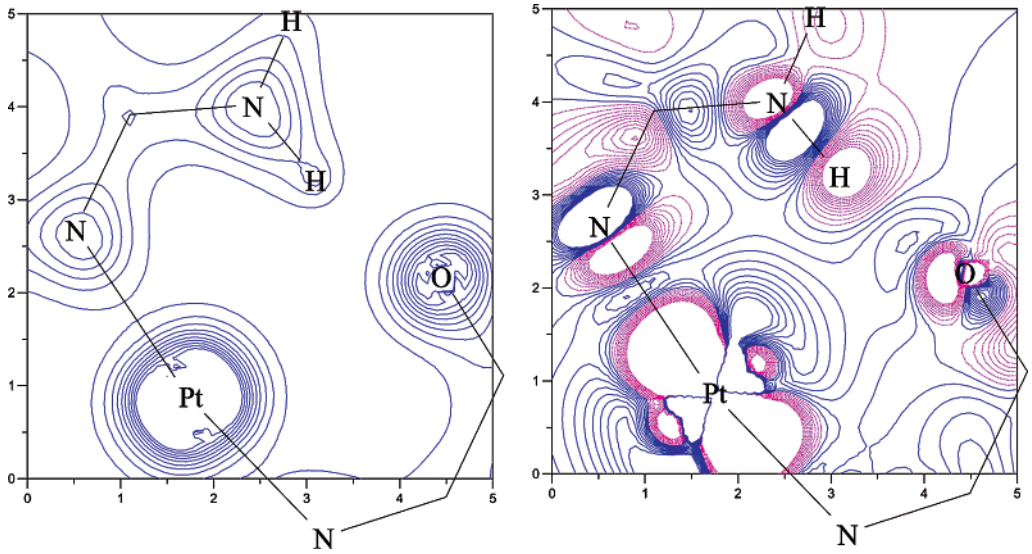

Figure 8. Electron density and the density difference ($\Delta\rho$) map in the plane of Pt−O6(G)−H4(C) of the N1 deprotonated complex. $\Delta\rho = \rho[(NH_3)_2PtGC^+] - \rho[(NH_3)_2Pt^{2+}] - \rho[G^-] - \rho[C]$, where G^- is the N1 deprotonated guanine. The increase of contour lines in the density map is at 0.1 au. Contours in the deformation density map at ±0.001 au. Dashed pink is for decrease of density, and solid blue is for increase of density.

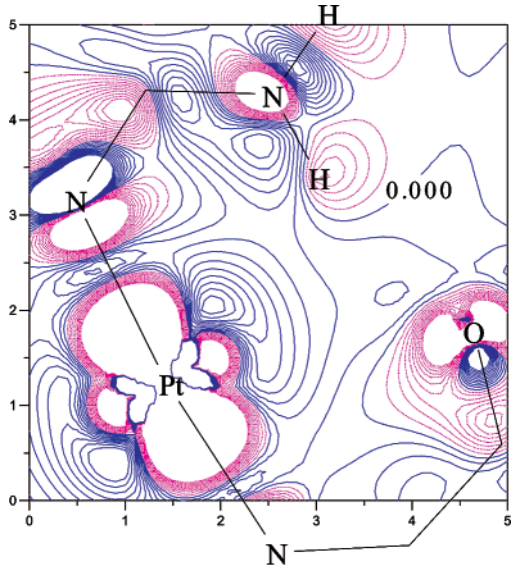

Figure 9. Electron density difference map $\Delta\rho = \rho[\{(NH_3)_2PtGC^+\}_2] - 2\rho[(NH_3)_2Pt^{2+}] - 2\rho[G^-] - 2\rho[C]$ in the plane of Pt−O6(G)−H4(C) of the platinated GCGC tetrad. Contours in the deformation density map at ±0.001 au. Dashed pink is for decrease of density, and solid blue is for increase of density.

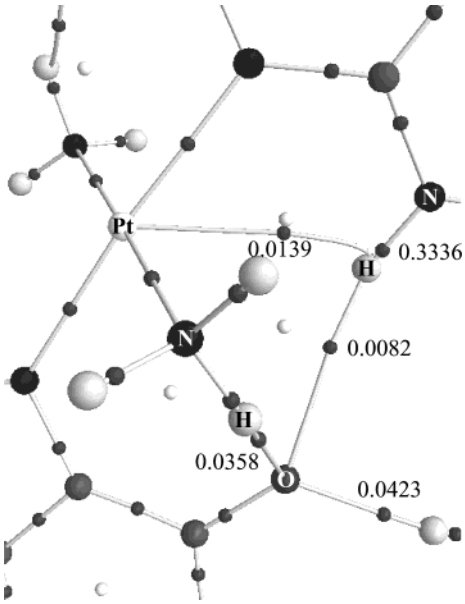

Figure 10. Density of bond critical points around the H4(C)···O6(G) H-bond and Pt in the platinated GCGC tetrad. The unit of density is in au. A curved bond path and a BCP with density of 0.0139 au can be seen between Pt and H4(C).

H4 of C and O6 of G (see Figure 8). Through this electron density increase, the deprotonation process at N1 of G reinforces the H4(C)···O6(G) H-bond. A similar effect of N1(G) deprotonation on the model **M2** is also apparent in its density difference map. The density variation between Pt^{2+} and O6(G) in monovalenced *trans*-$[(NH_3)_2Pt(G-N7)(C-N3)]^+$ has no substantial alternation compared to that of the divalenced parent complex. The density deformation between the complex and the deprotonated GC pair and the $(NH_3)_2Pt^{2+}$ moiety resembles the corresponding map in Figure 6. The deprotonation seems to have little influence on the Pt^{2+}− O6(G) interaction. The AIM analysis of the density at the BCPs of the deprotonated complexes reveals significant increases in density between the H4(C)···O6(G) H-bond (0.0465 vs 0.0221 au for model complex and 0.0393 vs 0.0130 au for platinum complex, respectively). Whereas, the density change at the BCP between $Pt^{2+}$and O6(G) has minor intensification (0.0178 vs 0.0125 au) (see Figure 7).

Influence of Dimerization on the H4(C)···O6(G) H-Bonding Pattern. Due to the dimerization, O6 of guanine is involved in three H-bonds: H(a1)···O6(G) (**R6**) (bond length of 1.865 Å), H4(C)···O6(G) (**R5**) (bond length of 2.279 Å), and H4(C′)···O6(G) (**R9**) (bond length of 1.770 Å) in the platinated GCGC tetrad (Figure 3). In the tetrad, the **R5** bond is approximately 0.07 Å longer than that in the platinated GC pair. This suggests that **R9** forms a stronger bond than **R5,** verifying that Pt^{2+} weakens the intra-base pair H-bonding H4(C)···O6(G).

The electronic structure of the H4(C)···O6(G) bond of the tetrad illustrated in Figure 9 displays the result of the formation of H4′(C′)···O6(G). The additional electron density around O6

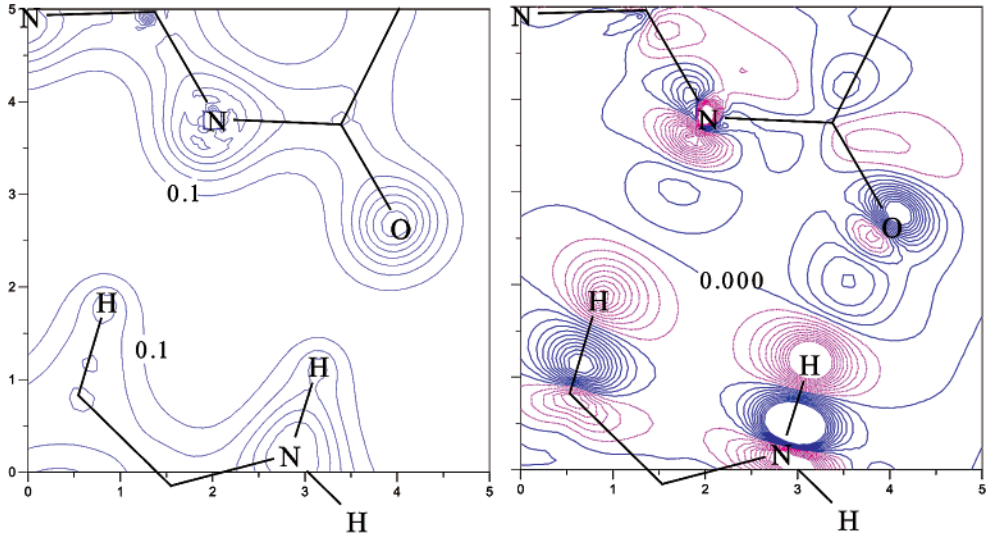

Figure 11. Electron density and the density difference map in the plane of H5(C)−N1(G)−H4(C) of the platinated GCGC tetrad. $\Delta\rho = \rho[\{(NH_3)_2PtGC^+\}_2] - 2\rho[(NH_3)_2PtGC^+]$. The increase of contour lines in the density map is at 0.1 au. Contours in the deformation density map at ±0.001 au. Dashed pink is for decrease of density, and solid blue is for increase of density.

covers two areas; one points to the H4 of cytosine in the GC pair and the other points to the H4′ of C from another GC pair. As compared to the electron structure of *trans*-$[(NH_3)_2Pt(G-N7)(C-N3)]^+$ (Figure 8), the formation of the second H-bonding interaction between O6(G) and H4′(C′) reduces the H4(C)···O6(G) H-bonding in the deprotonated monomer. Unlike the electronic structure found in *trans*-$[(NH_3)_2Pt(GH-N7)(C-N3)]^{2+}$ where the additional electron density is located between Pt and O6 (Figure 4), the density increase can still be found between H4 and O6. The interaction between Pt and O6 in the tetrad is expected to be weak. On the other hand, a significant increase in density can be seen between H4 and Pt in the platinated tetrad, suggesting a possible Pt···H4(C) interaction. This electron density property is in accordance with the Pt···H4(C) separation of 2.677 Å in the tetrad (2.725 Å in the base pair).

The AIM analysis of the BCPs of the complex suggests a weakened H4(C)···O6(G) H-bond (with density of 0.0082 au at the BCP) and a stable H4′(C′)···O6(G) H-bond (with density of 0.0423 au). It is important to note that the BCP between Pt and O6 that exists in the platinated GC pairs cannot be found in the tetrad. Instead, a bond critical point with density of 0.0139 au has been detected between Pt and H4(C) in the tetrad (Figure 10). Although the Pt···H4(C) atomic distance and its bond critical point characteristic are typical for a H-bond, the electronic structure in the density deformation map and the value of N4(C)−H−Pt atomic angle (113.7°) are not convincing that this is a H-bond.

Electronic Structure of the Unprecedented H5(C′)···N1(G) H-Bonding Pattern. Another unique feature of the platinated GCGC tetrad is that typical H-bonding geometric characteristics are derived for the H5(C′)···N1(G) atomic pair. As a corresponding model, the N7 protonated GCGC base tetrad (**M4**) has also been optimized at the B3LYP/6-311G(d,p) level of theory (Figure 3). However, the H5(C′)···N1(G) H-bonding pattern has not been observed for the model complex **M4** in which the H5(C′)···N1(G) separation amounts to 3.182 Å. Recent theoretical study of the microsolvation of guanine tautomers suggested that the formation of H-bonds at N1(G) and H7(G) greatly stabilizes the N1-deprotonated−N7-protonated guanine tautomer. Large H5(C)···N1(G) separation seems to suggest that the geometric constrains prevent the formation of H5(C)···N1(G) H-bond in **M4**.

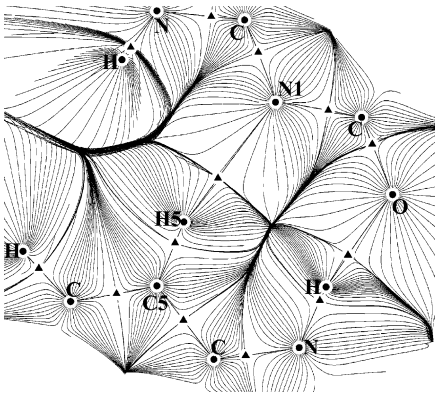

Figure 12. Gradient vector field of the charge density around the CH5(C)···N1(G) H-bond in the platinated GCGC tetrad. The bond critical points are in triangles.

The H-bond lengths between the platinated GC pairs predicted in the theoretical study have been found to be 1.770 Å (**R9**) and 2.288 Å (**R10**). The former corresponds to an N4′(C′)···O6(G) separation of 2.790 Å, about 0.08 Å longer than the corresponding crystallographic data (2.715 Å). For the latter, the H5(C′)···N1(G) bond distance seems to be 0.42 Å too short compared to the experimental measurement. However, if one adjusts the short H5(C)···C5(C) distance of 0.88 Å assumed in experiments to 1.080 Å (theoretical prediction), the experimental H5(C′)···N1(G) bond length should be adjusted to 2.51 Å, about 0.21 Å longer than the theoretical value. Considering that there is no counterion included in the calculation, the short theoretical H5(C′)···N1(G) H-bond length supports the proposal that the long H-bonding distances are essentially a consequence of the stacking effect of the counterion.[8] The C5(C′)−H−N1(G) bond angle of 161.3° evaluated at the B3LYP/AE level of theory also agrees well with the experimental value of 160°.

The electron density deformation map of the H5(C)···N1(G) H-bond in the metalated GCGC tetrad (Figure 11) illustrated a well-defined increase of electron density between H5 of C and

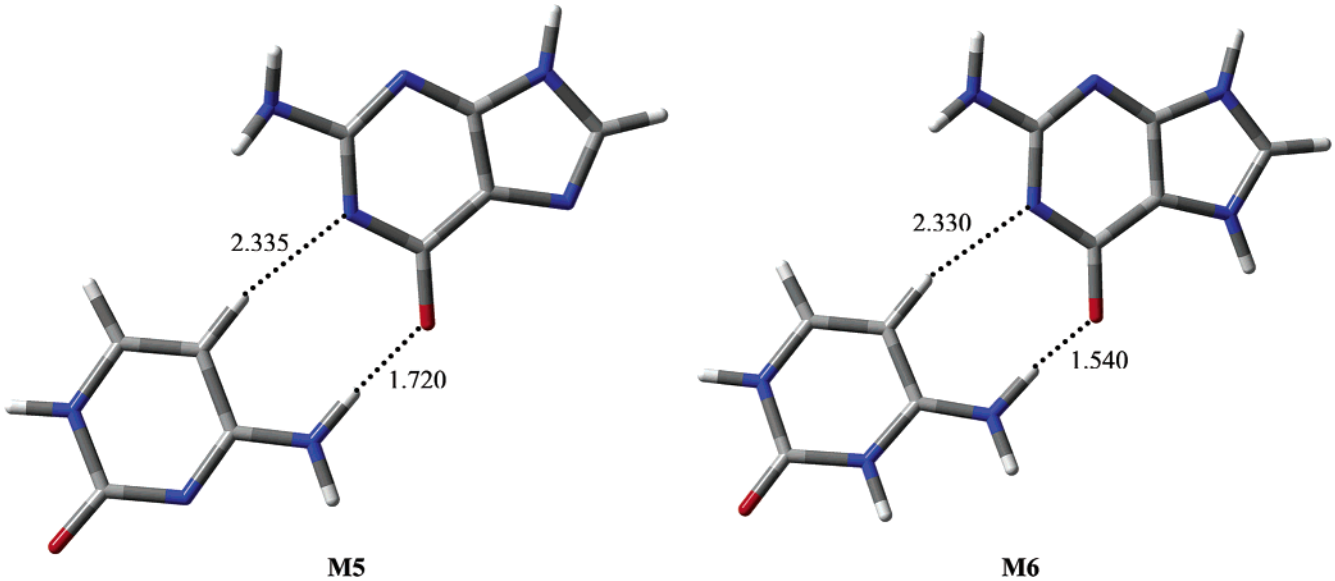

Figure 13. Optimized structure of the CH···N models **M5** and the diprotonated model **M6**. The representations of color at the atomic position are red for O, blue for N, gray for C, and white for H. Geometric parameters of the models are given in Å.

N1 of G. On the other hand, no density boost has been detected between the corresponding atoms in the model tetrad **M4**. The gradient vector field of the charge density around the H5(C)···N1(G) H-bond in the platinated GCGC tetrad is displayed in Figure 12. The trajectories of the gradient of density starting from H5(C) also follow the direction of the steepest ascent of the electron density deficiency surrounding the H5 of cytosine in Figure 11. The density value of 0.0154 au at the BCP between H5(C) and N1(G) signifies a moderate H-bond.

General Features of Electronic Structure of the CH···N H-Bonding Pattern. To explore the possibility of the CH···N H-bonding pattern between bases in general, a GC pair linked through H5(C)···N1(G) and H4(C)···O6(G) was optimized for comparison (Figure 13, **M5**). In this model, the H5(C)···N1(G) H-bond length amounts to 2.335 Å, 0.05 Å longer than that in the platinated GCGC tetrad. The C5(C′)-H−N1(G) bond angle of 163.4° in **M5** indicates strong H-bonding between H4(C) and O6(G). Two protons were added to N7 of G and N3 of C in the model base pair (**M6**) to mimic the charge influence of Pt on the H5(C′)···N1(G) H-bond in the platinated GCGC tetrad. The H5(C)···N1(G) bond length and the C5(C)−H−N1(G) bond angle have been computed to be 2.330 Å and 159.6°, respectively. Accordingly, the geometry of the H5(C)···N1(G) H-bond is not significantly influenced by the charge variation on the GC pair. In addition, platination seems to slightly increase the H5(C)···N1(G) H-bonding interaction as demonstrated by the shorter H5(C)···N1(G) H-bond distance of 2.288 Å.

The electron density deformation map of the **M5** and **M6** models exhibits the typical H-bonding characteristics for the H5(C)···N1(G) atomic pair. The density increase in **M5** is only slightly smaller than that in **M6**, which is consistent with the difference of their H-bond length. However, the electron density increase in **M6** is almost the same as that in the platinated GCGC tetrad. Therefore, the shorter H5(C)···N1(G) H-bond in the tetrad should be the result of the geometric constraints due to the platination of G and C in the tetrad. The electronic structure of the H5(C)···N1(G) H-bond is also not sensitive to the chemical alternation at the N site of the bases.

Table 2. Deprotonation Energy of the Platinated GC Pair and the Corresponding Models at the DFT Levels of Theory[a]

	ΔE
platinated GC pair	
AE	9.01
LANL2DZ	8.98
MWB	8.98
model	11.62
guanine	15.37

[a] Basis set used for nonmetal elements is 6-311G(d,p). $\Delta E = E\{[(NH_3)_2Pt(G-N7)(C-N3)]^+\} - E\{[(NH_3)_2Pt(GH-N7)(C-N3)]^{2+}\}$ in eV. Models and Guanines are calculated at the B3LYP/6-311G(d,p) level.

The density at this BCP in the **M5** and **M6** models is similar to that in the tetrad, 0.0148 au and 0.0145 au for **M5** and **M6**, respectively. This similarity confirms the observation that the electronic structure of the H5(C)···N1(G) H-bond is insensitive to the chemical alternation on the N sites.

Influence of Pt on the Deprotonation Energy of *trans*-$[(NH_3)_2Pt(GH-N7)(C-N3)]^{2+}$. The energy properties of the metalated GC pairs and the corresponding models are summarized in Table 2. The deprotonation energy of *trans*-$[(NH_3)_2Pt(GH-N7)(C-N3)]^{2+}$ has been evaluated to be 9.01 eV at the B3LYP/AE level of theory. For comparison, the deprotonation energy for the model GC pair and guanine base amounts to 11.62 and 15.37 eV, respectively, at the B3LYP/6-311G(d,p) level. Platination at the N7 of guanine considerably reduces the deprotonation energy. This result is consistent with the earlier experimental observations in solutions that the release of the protons from N1 of G is facilitated by the N7-coordinated cis-a_2Pt(II).[57] This significant reduction of deprotonation energy of guanine in the platinated complex should be attributed to the fact that part of the electron density of guanine transfers to the positively charged Pt(II), as can be seen from Mulliken population analysis.

The binding energy of the N-platinated GCGC base tetrad with respect to the two platinated GC pairs has been evaluated

(56) Hanus, M.; Ryhacek, F.; Kubar, R.; Bogdan, T. V.; Trygubendo, S. A.; Hobza, P. *J. Am. Chem. Soc.* **2003**, *125*, 7678−7688.
(57) Sigel, H.; Song, B.; Oswald, G.; Lippert, B. *Chem. Eur. J.* **1998**, *4*, 1053−1060.

to be 2.87 kcal/mol at the B3LYP/AE level (3.98 kcal/mol at the B3LYP/LANL2DZ level and 3.78 kcal/mol at the B3LYP/MWB level). However, this small binding energy does not represent the H-bonding energy between the platinated GC pairs because both pairs are positively charged and no counterions are taken into account in the calculations. A charge repulsion model calculation with two single-charged particles at the distance of two Pt's in the tetrad demonstrates that the charge repulsion energy in this system is as high as 39.69 kcal/mol. Therefore, the H-bonding energy between two platinated GC pairs amounts to 42.56 kcal/mol, signifying a quite strong bonding energy for the C−H5(C)···N1(G) type H-bond. A detailed analysis for the bonding energy of the unique bonding pattern in the plantinated base pairs and base tetrads will be reported elsewhere.

Conclusions

The consistency of the geometric parameters predicted with the different basis set and the good agreements compared to the crystallographic data ensure the high quality and reliability of the levels of calculations used in the study.

The application of electronic structure analysis and the AIM calculations reveals the details of the H-bonding pattern and the influence of metalation in the base pair and base tetrad. The influence of Pt on the intra base pair H-bonding can be summarized as follows. When the electron density on the O6 of guanine is large, Pt tends to interact with O6. Otherwise, it actively interacts with the proton at the N4 site of cytosine. The overall effect of Pt is to reduce the intra base pair H-bonding of N4(C)···O6(G) in the platinated GC pair or GCGC tetrad.

The relaxation of geometry constraints in metalated nucleobases is decisively important in the formation of novel molecular architectures from nucleobases and metal entities. The incorporation of the platinum in the GCGC tetrad benefits the formation of the unique CH···N (H5(C)···N1(G)) hydrogen bond in the tetrad by offering improved geometric constraints rather than by changing the electronic properties around the H5(C) and N1(G) sites.

The existence of the C−H···N type H-bond does not depend on the metalation of the nucleobases. The electronic structure of the C−H···N H-bond is not affected by the chemical alternation or the electronic properties at the N7 site of guanine and the N1 site of cytosine in the base pair. The H-bonding energy of the C−H···N type H-bond is expected to be similar to that of the N−H···N type.

Platination at the N7 of guanine reduces the deprotonation energy considerably. The deprotonation energy of the divalenced platinum complex *trans*-$[(NH_3)_2Pt(GH-N7)(C-N3)]^{2+}$ has been evaluated to be 9.01 eV. For comparison, the deprotonation energy for the model GC pair and guanine base monomer amounts to 11.62 and 15.37 eV, respectively.

Acknowledgment. This research project in the PRC was supported by the "Knowledge Innovation Program" and the "Introducing Outstanding Overseas Scientists Project," Chinese Academy of Sciences. In the United States the project was supported by the ONR Grant No. N00014-98-1-0592,the NIH SCORE Grant No. 3-S06 GM008047 31S1 and NSF CREST Grant No. HRD-0318519.

Supporting Information Available: Tables of optimized geometric parameters, energy properties of the platinated GC pair and the corresponding models, DFT/AE optimized *x*,*y*,*z* coordinates, and Mulliken population analysis. Figures of electron density difference maps. This material is available free of charge via the Internet at http://pubs.acs.org.

JA0492337